Iron normal mode dynamics in a porphyrin-imidazole model for deoxyheme proteins

Brajesh K. Rai,[1] Stephen M. Durbin,[1] Earl W. Prohofsky,[1] J. Timothy Sage,[2] Mary K. Ellison,[3] W. Robert Scheidt,[3] Wolfgang Sturhahn,[4] and E. Ercan Alp[4]

[1]*Department of Physics, Purdue University, West Lafayette, Indiana 47907*

[2]*Department of Physics, Northeastern University, Boston, Massachusetts 02115*

[3]*Department of Chemistry and Biochemistry, University of Notre Dame, Notre Dame, Indiana 46556*

[4]*Advanced Photon Source, Argonne National Laboratory, Argonne, Illinois 60439*

(Received 20 June 2002; published 12 November 2002)

Iron vibrational modes of a deoxyheme protein model (2-methylimidazole)(tetraphenylporphinato)iron(II), [Fe(TPP)(2-MeImH)], have been studied by refining normal mode calculations to nuclear resonance vibrational spectroscopy (NRVS) data. The NRVS measurements give quantitative frequencies and iron amplitudes of all modes with significant Fe vibrational motion. Modes with in-plane displacement of iron are distinguished from those involving out-of-plane motion by measurements on oriented single-crystal samples. Normal modes having large overlaps with in-plane ν_{42}, ν_{50}, and ν_{53} modes of the porphyrin core are identified, as well as several modes with large iron-imidazole stretch components. An out-of-plane mode at 78 cm^{-1} shows significant doming of the porphyrin core, but the largest Fe doming motion arises from the coupling of phenyls and imidazole at 25 cm^{-1}.

DOI: 10.1103/PhysRevE.66.051904 PACS number(s): 87.15.Aa, 87.64.Bx

I. INTRODUCTION

Myoglobin and hemoglobin are examples of proteins containing heme molecules that perform their biochemical functions by reversibly binding and releasing diatomic ligands, including O_2, CO, and NO, at the heme iron active site [1,2]. Vibrational analyses of heme proteins and model heme compounds have led to fairly detailed descriptions of vibrational modes in the high frequency range between 1200 and 1600 cm^{-1} [3–5]. These modes serve as reliable indicators of iron spin, oxidation, and ligand states, and are readily observed by resonance Raman and infrared (IR) optical techniques. The high frequency heme modes are due to the localized vibrations of the porphyrin core, which largely do not involve motion of the Fe atom, and hence give little direct insight into the role of iron dynamics in important biological reactions.

A direct measurement of biologically significant iron modes (e.g., the low frequency modes involving large amplitude motion of iron) is hindered by optical selection rules associated with the traditional Raman and IR methods. In particular, the E_u and A_{2u} normal modes of a D_{4h} symmetric porphyrin, the only modes that involve nonzero displacements of iron, are Raman inactive [3,4]. Ligand and porphyrin isotope substitution combined with the Raman or IR methods to characterize heme normal modes works well for high frequency vibrations, but is less effective at lower frequencies. Substitution of ^{54}Fe for ^{57}Fe helped to determine the correct assignment of the iron-histidine mode in myoglobin, but was not sensitive enough to identify any other Fe mode [6,7].

Some of the shortcomings of optical techniques for observing iron vibrational modes can be overcome with nuclear resonance vibrational spectroscopy (NRVS), which in principle can determine all modes having significant iron motion [8–10]. NRVS measures the frequencies and amplitudes of all iron modes over a wide energy range ($\sim$0–800 cm^{-1}), and directional information is possible with crystalline specimens. Measured frequencies, amplitudes, and directions of iron atom motions provide many more constraints for normal mode calculations, permitting a realistic description of Fe normal modes. In a recent study using NRVS and normal mode analysis, Rai *et al.* identified several biologically important iron modes of heme model compound (nitrosyl)iron(II) tetraphenylporphyrin, [Fe(TPP)(NO)] [11]. Using NRVS, iron dynamics in [Fe(TPP)(NO)] [12] and myoglobin [13] were also studied by Sage and coworkers. Further NRVS studies of Mb were recently published by Achterhold *et al.* [14].

We present here a complete iron vibrational spectrum of a deoxyheme model compound, (2-methylimidazole)(tetraphenylporphinato)iron(II), [Fe(TPP)(2-MeHIm)], using NRVS data and normal mode analysis. This compound closely models the heme structure in myoglobin and hemoglobin, where the iron atom is bound to the imidazole ring of a histidine residue in the protein. The NRVS measurements cover an energy range of $\sim$0–700 cm^{-1}, where most iron vibrations are expected to occur. The data were acquired from a polycrystalline powder as well as oriented single-crystal samples, which are essential for distinguishing between heme in-plane and out-of-plane modes. By refining the force fields for normal mode analysis, excellent agreement between the measured and calculated iron vibrational density of states (VDOS) is achieved. This calculation provides a detailed description of all normal modes of this molecule, allowing the contributions of the imidazole ring and the substituent phenyls to be fully characterized.

II. METHODS

A. Sample preparation

Synthesis and isolation of [^{57}Fe(TPP)(2-MeHIm)] 1.5C_6H_5Cl. All reactions and manipulations were done using standard Schlenkware techniques. Benzene was distilled over

sodium benzophenone and ethanethiol (Aldrich) was used as received. Chlorobenzene was washed with concentrated sulfuric acid, then with water until the aqueous layer became neutral, then dried with $MgSO_4$, and distilled twice over P_2O_5 under argon. 2-Methylimidazole was purchased from Aldrich, recrystallized from toluene (or methanol), and dried under vacuum. *Meso*-tetraphenylporphyrin (H_2TPP) was prepared according to Adler *et al.* [15]. ^{57}Fe-enriched [Fe(TPP)Cl] (95%) was prepared according to the metallation procedure of Landergren and Baltzer [16]; $[^{57}Fe(TPP)]_2O$ was prepared from [^{57}Fe(TPP)Cl] [17]. [^{57}Fe(II)(TPP)] was prepared by reduction of $[^{57}Fe(TPP)]_2O$ (65 mg, 0.04 mmol) with ethanethiol ($\sim$1 mL) in benzene according to Stolzenberg *et al.* [18]. The benzene solution was stirred overnight followed by solvent removal under vacuum. The solid [^{57}Fe(II)(TPP)] was never exposed to air to avoid the easily formed $[Fe(TPP)]_2O$.

[^{57}Fe(TPP)(2-MeHIm)]1.5C_6H_5Cl was prepared by adding via cannula transfer excess 2-methylimidazole (32 mg, 0.40 mmol) in 15 mL of dry degassed chlorobenzene to solid [^{57}Fe(II)(TPP)] and stirred for 15 min. The solution was carefully transferred via cannula to several 8 mm$\times$250 mm glass tubes. Hexanes (distilled over sodium benzophenone) were layered over the solution for the liquid diffusion experiment. The tubes were flame-sealed. Large x-ray quality crystals were obtained after 2 weeks. Powder specimens were prepared from the same starting material used for growing crystals.

Crystals of [^{57}Fe(TPP)(2-MeHIm)]1.5C_6H_5Cl were isolated and mounted in an inert-atmosphere dry box. A single dark purple crystal (1.7 mm$\times$0.7 mm$\times$0.6 mm) of [^{57}Fe(TPP)(2-MeHIm)]1.5C_6H_5Cl was used for the experiment. The crystal was mounted in a 2-mm-diameter, thin-walled (0.01 mm), boron-rich, X-ray diffraction capillary tube that was purchased from the Charles Supper Company. The crystal was immobilized in the capillary tube with a small amount of Dow Corning high-vacuum grease. The capillary tube was sealed and secured to a small length of 18-gauge copper wire with epoxy. The copper wire was then secured with epoxy to a brass mounting pin. The copper wire allowed for enough flexibilty to make minor adjustments in the orientation of the crystal. The brass mounting pin, holding the crystal, was then mounted on a eucentric goniometer head to allow for further fine adjustments in the orientation of the crystal.

Crystals of [Fe(TPP)(2-MeHIm)]1.5C_6H_5Cl are known to crystallize in the triclinic system with two molecules per cell related by inversion symmetry [19]; thus there is only one orientation of the porphyrin plane in the single crystal. This solid-state feature allows the best arrangements for the oriented NRVS experiments, which is to have the porphyrin planes parallel or perpendicular with respect to the incident beam. This requires that the crystal be aligned so that only a crystal rotation about the goniometer head axis is necessary to obtain sample orientations with the porphyrin plane parallel and perpendicular to the beam. The $(\bar{2}08)$ Bragg plane is the crystallographic plane parallel to the mean porphyrin plane. A drawing of the view normal to the $(\bar{2}08)$ face confirmed that indeed the porphyrin plane is coplanar with the $(\bar{2}08)$ plane. Defining this orientation was done by determining the unit cell constants and noting the orientation of $[\bar{2}08]$ with a binocular microscope. The $[\bar{2}08]$ direction must be made perpendicular to the goniometer rotation axis. Since the shapes of the [^{57}Fe(TPP)(2-MeHIm)]1.5C_6H_5Cl crystals are irregular, the crystal was brought to this convenient orientation by trial and error which meant remounting the crystal in the dry box after determining the corrcct orientation using the diffractometer as described above. Final rough adjustments were made by bending the copper wire so that the crystal orientation was within $\pm 10°$ to the goniometer axis. Finally the position of the crystal could now be adjusted using the angle adjustments on the eucentric goniometer head. This position and a 90° rotation around the goniometer axis give the two desired orientations. The position of the crystal was rechecked after the beam line experiments and showed that the crystal had changed position by less than 0.3°.

B. Nuclear resonance vibrational spectroscopy

NRVS is a technique that employs the unique capabilities of advanced x-ray synchrotron sources. It utilizes the Mössbauer transition in certain nuclear isotopes to observe shifts in the nuclear absorption probability caused by vibrational motions of the nuclei, from which the partial vibrational density of states can be determined. The current study is restricted to the ^{57}Fe isotope.

An x-ray can be resonantly absorbed by the nucleus when the x-ray energy E_x is within the exceedingly narrow Mössbauer linewidth (about 10^{-8} eV) of the resonance ($E_o \approx 14.413$ keV). If the difference between E_x and E_o matches the energy of a vibrational quantum of the system E_{vib}, however, absorption can occur; e.g., if $E_x + E_{vib} = E_o$. Classically this is analogous to a Doppler shift, where the moving nucleus sees a Doppler-shifted x-ray energy changed from E_x to E_o.

There are two critical properties of the x-ray beam, which require a specialized beam line at a third-generation x-ray synchrotron: there must be a sufficiently large number of x-ray photons within the 10^{-8} eV bandwidth to excite acceptable count rates, and this excitation beam must have an energy bandpass about E_x which is narrower than typical vibrational energies; about 1 meV (or 8 cm^{-1}) is desirable. For the studies reported here, samples contained about 10^{18} resonant Fe atoms, and data collection required 2–4 h. (The natural ^{57}Fe concentration of 2.4% was enriched to over 90% in these samples, an essential step for reasonable data collection times.)

Iron dynamics are probed by measuring the x-ray absorption spectrum over a typical energy range of 0–700 cm^{-1} about the resonance. By scanning the x-ray energy both below and above the resonance energy E_o, the Stokes and anti-Stokes components of the absorption spectrum are obtained. This provides a direct measure of the sample temperature, and allows for the extraction of the Fe partial vibrational density of states [10]. Further details of the NRVS

technique have been described elsewhere [8,9,12,20,21].

All measurements were conducted at the SRI-CAT sector 3-ID-D station of the Advanced Photon Source, Argonne National Laboratory. The single crystal was positioned in the incident x-ray beam so that the beam was either parallel or perpendicular to the heme plane, within $\approx \pm 2°$. The capillary tube containing the crystal was directly exposed to a stream of cold N_2 gas from a source of liquid nitrogen, sufficient to cool the crystal to 110 K as directly determined from the NRVS data. The powder specimen was prepared by mixing it with a small amount of vacuum grease and placing in a sealed cell that was directly mounted onto a He flow cryostat. Data were obtained at 20 K for this polycrystalline sample. For both the crystal and the powder specimens, resonant absorption of the incident x rays was monitored by Fe *K* fluorescence observed with a time-resolving Si avalanche photodiode detector.

C. Computational details

Normal mode calculations on [Fe(TPP)(2-MeHIm)] model were performed in a mass-weighted Cartesian coordinate system. The structural parameters for the model were taken from the x-ray measurements of Ellison *et al.*, which were slightly modified to keep the structures of each of the four pyrroles and phenyls identical [19]. This structure consists of 83 atoms, of which 77 make up the Fe(TPP) molecule and the remaining 6 atoms form the imidazole ring (Fig. 1). The hydrogen atoms of the pyrrole and phenyl rings were explicitly included, and the four pyrrole rings are constrained to be coplanar, with the phenyls oriented perpendicular to the pyrrole plane. The methyl group of the imidazole was replaced by a point mass of 15 amu and the imidazole hydrogens were taken to be the part of the atom to which they are bound. In agreement with the x-ray data, the central Fe atom was positioned 0.4 Å below the porphyrin plane, towards the imidazole ring. Also in accordance with the observed x-ray structure, the Fe-N_{im} bond was oriented 8° off the heme normal, and the imidazole ring assumed an asymmetrical position with respect to the Fe-N_{im} bond (Fig. 1).

The potential energy of the [Fe(TPP)(2-MeHIm)] system was expressed using the Wilson-type force fields which included bond stretch, angle bend, torsion, and out-of-plane bend force constants [22]. In addition to these force constants, which correspond to the diagonal terms in the force constant matrix, the stretch-stretch, stretch-bend, and bend-bend interactions related to the off-diagonal terms in the force constant matrix were also included. The initial set of force constants for the porphyrin core and the phenyls were transferred from earlier works on [Fe(TPP)(NO)] by Rai [11] and [Ni(TPP)] by Rush [23]. Initial unrefined imidazole force constants were obtained from a previous study of Eyster [24].

The normal mode calculation using the initial force constants gave an iron VDOS which were in rough agreement with the observed spectrum. The initial force fields of the [Fe(TPP)(2-MeHIm)] system were then refined to improve the match between the calculated and observed iron VDOS,

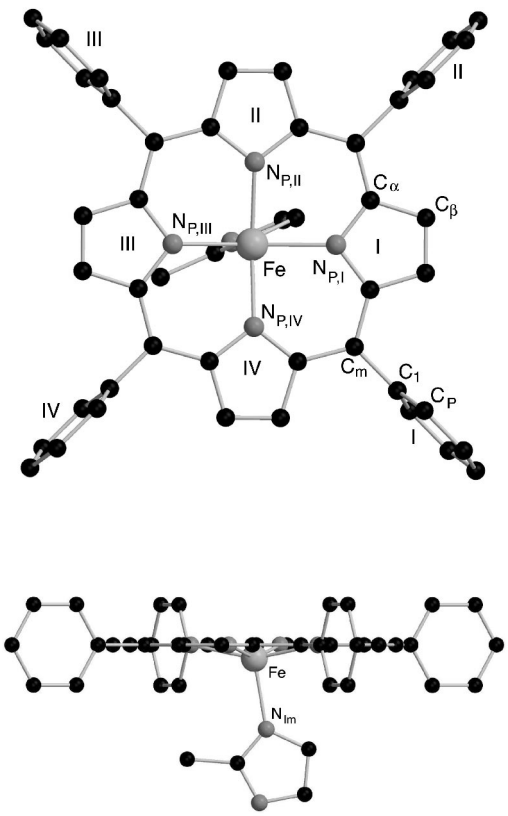

FIG. 1. Structure of the model [Fe(TPP)(2-MeHIm)], top (top) and side (bottom) views. Notice that the iron is pulled out of the porphyrin plane, towards the imidazole ring. The Fe-N_{im} bond is tilted 8° off the heme normal. For clarity, the beta hydrogens and the hydrogen atoms on the phenyl rings have been omitted.

using the Jacobian-determinant method [25]. In addition, several force constants were also adjusted manually to get a better fit of the calculated iron spectrum to that obtained experimentally. These included off-diagonal force constants, e.g., the coupling between vibrations of nearby bonds [22].

In order to get an acceptable fit of our calculation to the experimental data, several diagonal (stretch, angle bend, torsion, and out-of-plane bend) and off-diagonal (interaction) force constants were adjusted. Only a small subset of our best-fit stretch force constants were different from those reported for NiTPP [23]. The biggest change was for the four Fe-N_P bond stretches, which were (on an average) 30% smaller than the corresponding Ni-N_P values. This is expected, as a replacement of Ni by Fe will significantly affect the electron orbital overlaps of the central atoms with pyrrole nitrogens, causing a major change in these force constants. For a few other stretch force constants, this difference was under 2%, and a majority of the stretch force field values remained unchanged at the end of the refinement.

Similarly, the refinement of the angle bend force fields resulted in larger changes of those bending force constants that involve the iron atom. The N_P-Fe-N_P and C_α-N_P-Fe angle bend force constants were changed by -70% and $+30\%$, respectively, from their values in NiTPP. The adjustments required for approximately half of the remaining angle bend force constants were within 20% of their values in

NiTPP, and the rest of the angle bend values did not change.

The out-of-plane force constants (torsions and out-of-plane bends), which are in general one to two orders of magnitude smaller than a typical stretch force constant, were also refined. All of the refined out-of-plane force constants were in a physically reasonable range of 0.01–0.4 mdyn Å/rad^2. Only a minor tweaking in the interaction force constants was needed in the refinement. In most cases these interaction force constants are small, and are roughly one-tenth of the average of the corresponding diagonal force constants.

In addition to the transferred force constants for the porphyrin phenyl [23] and the imidazole units [24], a complete description of this system must include the coupling of the porphyrin with the imidazole. We introduced initial estimates for the Fe-N_{im} stretch and N_P-Fe-N_{im} bend force constants, for example. These coupling force constants were subsequently adjusted during the refinement. Overall, refinement gave physically meaningful changes in the force field, and none of our force constants assumed unreasonable values.

We apply the procedure described by Rai *et al.* [11] to calculate the Fe vibrational density of states of [Fe(TPP)(2-MeHIm)], which is then compared with the experimental iron VDOS. The results from normal mode analysis are used to calculate first the nuclear absorption probability and subsequently the iron VDOS. The normalized mass-weighted eigenvector of each mode is transformed and projected out to give iron amplitudes in Cartesian coordinates. The one-phonon contribution to the absorption probability, $S_1(E,\hat{k})$, is obtained using the frequency and iron amplitude $(\vec{u})$ of each vibrational mode. At low temperatures, multi-phonon contributions to the nuclear absorption probability are negligible and can be ignored. The incident wave vector is represented by $\vec{k}$, and E indicates the difference between the energy of the incident radiation and the nuclear resonance energy of ^{57}Fe. The one-phonon absorption probability is expressed as [26,27]

$$S_1(E,\hat{k}) = e^{-\langle(\vec{k}\cdot\vec{u})^2\rangle}\sum_{l=1}^{L} e^{\beta E_l/2}\frac{\Gamma/2\pi}{(E-E_l)^2+\Gamma^2/4}\prod_{j=1}^{L} I_{n_j}(C_j(\hat{k})), \tag{1}$$

where L is the total number of Fe modes, β is $1/kT$ (k is the Boltzmann's constant and T is the absolute temperature), and I_{n_j} is the Bessel function of the first kind of order n_j. E_l is the energy of the lth vibrational mode. Γ is the linewidth of vibrational transition and its value was set to 8 cm^{-1}, corresponding to the experimental energy resolution. In order to calculate one-phonon absorption probability, we set $n_j = \delta_{lj}$. The argument $C_j(\hat{k})$ of the Bessel function is defined as

$$C_j(\hat{k}) = \frac{\langle(\vec{k}\cdot\vec{u_j})^2\rangle}{\cosh(\beta E_j/2)}. \tag{2}$$

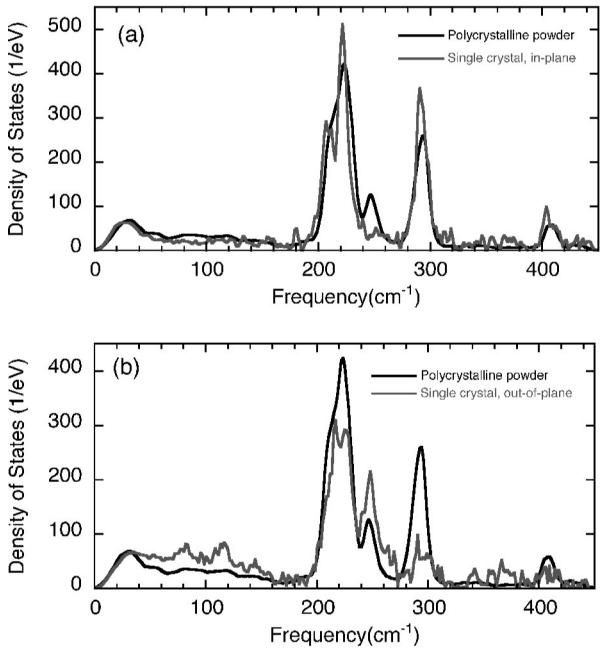

FIG. 2. Measured NRVS spectra of the polycrystalline powder sample and single crystals of [Fe(TPP)(2-MeIm)]. (a) Crystal oriented with heme planes parallel to the incident beam. (b) Crystal heme planes perpendicular to the incident beam. The measurements covered an energy range of ~0–700 cm^{-1}. However, the iron VDOS are reported only between 0 and 450 cm^{-1}. No distinct feature was noticed above 450 cm^{-1} in any of the measurements.

The Fe VDOS is directly related to the one-phonon absorption probability [9,26]

$$D(E) = 3\frac{E}{E_R}\frac{S_1(E)}{f}[1-e^{-\beta E}], \tag{3}$$

where E_R(=1.96 meV) is the recoil energy of ^{57}Fe nucleus and f is the Lamb-Mössbauer factor. Using Eq. (3) along with Eqs. (1) and (2), we calculate the Fe vibrational density of states, which is then compared to the experimental iron VDOS.

III. EXPERIMENTAL RESULTS

The measured vibrational spectrum from polycrystalline [Fe(TPP)(2-MeHIm)] was converted to iron vibrational density of states and is shown in Fig. 2. In order to distinguish between the heme in-plane and out-of-plane modes, two sets of measurements were made on an oriented single crystal, corresponding to parallel and perpendicular orientations of the heme planes with respect to the incident x-ray beam. Figures 2(a) and 2(b) show the iron VDOS of [Fe(TPP)(2-MeHIm)] in these two orientations, along with the polycrystalline data. With the x-ray beam parallel to the heme plane, the interaction with iron in-plane modes is enhanced and at the same time the out-of-plane modes are suppressed. Figure 2(a) clearly shows the presence of heme in-plane modes near 220, 290, and 400 cm^{-1}. On the other hand, an incident x-ray beam perpendicular to the heme plane increases the interaction with out-of-plane modes while suppressing in-plane vibrations. Several heme out-of-plane modes are readily identified from Fig. 2(b), e.g., at 214 and 248 cm^{-1}.

TABLE I. Percentage overlap of calculated modes with porphyrin core normal modes and ligand vibrations. The numbers indicate the scalar product of true [Fe(TPP)(2-MeHIm)] normal modes with the model eigenvectors corresponding to γ, ν, or ligand vibrations. The "Assignment" label is only an approximate guideline, as most modes are mixtures of multiple porphyrin core modes. No assignment is made if there is no dominant core mode. Low frequency modes assigned as phenyl or phenyl-imid have motions dominated by the substituents, as opposed to the porphyrin core modes.

Freq (cm^{-1})	Assignment	γ_9	γ_6	ν_{42a}	ν_{42b}	ν_{50a}	ν_{50b}	ν_{53a}	ν_{53b}	$\nu_{FeN_{Im}}$	$\delta_{FeN_{Im}C_{Im}}$
25	phenyl-imid	1	21	3	5	7	3	8	3		28
32	phenyl-imid	8	12	6		5	6	6	7		6
33	phenyl-imid	21	22		3	2	6	2	7	3	14
54	phenyl	4	2	4	1	12	12	8	8		3
56	phenyl		9	1	9	11	12	8	8		2
67	γ_9	29	15				1	1	1	4	11
79	γ_9	40	23			1		1		8	11
110	$\delta_{\text{Fe-imid}}$	22	19		3		1	3	8	5	44
191			4	8	3	2	5	15	8	4	9
213		3	15	13	12	8	6	5	10	25	9
215	$\gamma_6+\nu_{\text{Fe-imid}}$	1	76	5	3	8	4	5	2	63	1
222	$\nu_{42,53}$		4	15	10	4		5	21	2	1
224	$\nu_{42,53}$		2	25	9	3	5	26	12	1	1
225	$\nu_{42,53}$	3		10	42	6	4	25	26	20	8
228	$\gamma_9+\nu_{\text{Fe-imid}}$	18	4	6	19	1		12	11	39	3
248	$\gamma_9+\nu_{\text{Fe-imid}}$	40	12	2	12	5	7	3	3	52	6
288	$\nu_{50,53}$		1	13	1	35	23	39	27	1	4
293	$\nu_{53,50}$	3	2	17	3	24	35	25	39	5	7
404	$\nu_{50a,53a}$			7	7	70	1	20			1
406	$\nu_{50b,53b}$			8	8	1	70		20		5

Thus a comparison of the NRVS parallel and perpendicular spectra enables us to distinguish between the in-plane and out-of-plane modes, giving a direct experimental determination of the direction of the Fe displacement for various modes.

IV. COMPUTATIONAL RESULTS AND DISCUSSION

The normal mode analysis of a single molecule of [Fe(TPP)(2-MeHIm)] with 83 atoms gives 243 nonzero eigenvalues. For the purpose of analysis, the normal modes of this system can be categorized on the basis of their overlap with one of the three distinct structural units of the system, the porphyrin core, the phenyl rings, and the imidazole ligand. Iron dynamics will be most directly affected by the vibrations of the porphyrin core, while purely localized vibrations of the phenyl and imidazole rings will have negligible effect. However, the coupling of phenyl or imidazole motions with the porphyrin core do activate additional modes with significant iron motion, as we shall describe below.

We first consider the classification scheme for D_{4h} symmetric porphyrin, developed by Abe and co-workers [28]. For a 37-atom porphyrin core, the in-plane and out-of-plane modes can be classified as

$$\Gamma_{in\text{-}plane}=9A_{1g}+8A_{2g}+9B_{1g}+9B_{2g}+18E_u \qquad (4)$$

and

$$\Gamma_{out\text{-}of\text{-}plane}=3A_{1g}+6A_{2u}+5B_{1u}+4B_{2u}+8E_g, \qquad (5)$$

where Γ is the representation matrix. A nonzero displacement of Fe occurs only for E_u (in-plane) and A_{2u} (out-of-plane) modes, both of which are Raman inactive. The presence of an off-axial imidazole ligand lowers the symmetry of the otherwise fourfold symmetric porphyrin, which may make some of the E_u or A_{2u} modes Raman active (perhaps weakly). Most of these nominally inactive porphyrin modes, however, have not been identified in Raman measurements on various deoxyheme proteins and related porphyrin compounds, which suggests that the D_{4h} symmetry group might still have some relevance to the larger molecule considered here.

The classification scheme of the porphyrin core modes defines a complete orthonormal basis set (for the porphyrin core) of in-plane (ν_1 to ν_{53}) and out-of-plane modes (γ_1 to γ_{26}). However, due to mixing of imidazole and phenyl modes with porphyrin core vibrations, the individual normal modes of the [Fe(TPP)(2-MeHIm)] molecule are found to overlap with a number of ν_i and γ_i modes. The overlap of [Fe(TPP)(2-MeHIm)] normal modes with the porphyrin core modes is calculated by first constructing normalized mass-weighted vectors representing normal coordinates (ν_1 to ν_{53} and γ_1 to γ_{26}) of the porphyrin core basis set. The [Fe(TPP)(2-MeHIm)] normal modes are then classified by taking the inner product of the calculated eigenvectors with the eigenvectors of the porphyrin core basis set. Any mode

TABLE II. Frequencies of the observed and calculated modes, mode assignments, Fe amplitudes (at $T=20$ K), and potential energy distribution (PED). The in-plane and out-of-plane motions of Fe are indicated by ip and op, respectively. The contribution to the potential energy of a particular normal mode from stretch (ν), angle bend (δ), and torsion (τ), force constants is shown. The number in the bracket indicates the percentage contribution of a given force constant to the PED of the mode. Only those force constants that contribute 5% or more to the PED are listed.

Cal Freq. (cm^{-1})	Mode Assignment	Fe Ampl (pm)	PED(%)
25	phenyl-imid,op	3.45	$\delta_{FeN_{Im}C_{Im}}(33)+\delta_{N_{P,II}FeN_{Im}}(10)+\delta_{N_{P,III}FeN_{Im}}(11)+\delta_{N_{P,IV}FeN_{Im}}(15)$
32	phenyl-imid,op	1.97	$\delta_{N_{P,I}FeN_{Im}}(10)+\delta_{N_{P,II}FeN_{Im}}(15)+\delta_{N_{P,III}FeN_{Im}}(17)$
33	phenyl-imid,op	2.11	$\delta_{N_{P,I}FeN_{Im}}(22)+\delta_{N_{P,II}FeN_{Im}}(8)$
54	phenyl,ip	1.2	$\delta_{C_\alpha C_{m,II}C_2}(18)+\delta_{C_\alpha C_{m,IV}C_4}(15)+\tau_{C_{m,II}C_2C_{P,II}C_{P,II}}(12)+\tau_{C_{m,IV}C_4C_{P,IV}C_{P,IV}}(11)$
56	phenyl,ip	1.22	$\delta_{C_\alpha C_{m,I}C_1}(19)+\delta_{C_\alpha C_{m,III}C_3}(19)+\tau_{C_{m,I}C_1C_{P,I}C_{P,I}}(12)+\tau_{C_{m,III}C_3C_{P,III}C_{P,III}}(13)$
67	γ_9,op	1.26	$\delta_{FeN_{Im}C_{Im}}(15)+\delta_{N_{P,III}FeN_{Im}}(5)+\delta_{N_{P,IV}FeN_{Im}}(9)$
79	γ_9,op	1.51	$\nu_{FeN_{Im}}(9)+\delta_{FeN_{Im}C_{Im}}(13)+\delta_{N_{P,I}FeN_{Im}}(6)+\delta_{N_{P,II}FeN_{Im}}(9)$
110	$\delta_{\text{Fe-imid}}$,op	0.91	$\delta_{FeN_{Im}C_{Im}}(62)+\delta_{N_{P,I}FeN_{Im}}(7)+\delta_{N_{P,II}FeN_{Im}}(5)$
191	ip	1.24	$\tau_{C_{Im}N_{Im}C_{Im}C_{Im}}(34)+\tau_{N_{Im}C_{Im}C_{Im}N_{Im}}(14)$
213	ip,op	2.03	$\nu_{FeN_{P,II}}(6)+\nu_{C_{m,II}C_2}(8)+\nu_{C_{m,IV}C_4}(6)$
215	$\gamma_6+\nu_{\text{Fe-imid}}$,op	1.73	$\nu_{FeN_{Im}}(35)$
222	ip	1.16	$\nu_{FeN_{P,II}}(5)+\nu_{FeN_{P,III}}(17)+\nu_{FeN_{P,IV}}(13)$
224	$\nu_{42,53}$,ip	1.71	$\nu_{FeN_{P,I}}(9)+\nu_{FeN_{P,II}}(16)$
225	$\nu_{42,53}$,ip	1.63	$\nu_{FeN_{P,I}}(13)+\nu_{FeN_{P,IV}}(7)$
228	$\gamma_9+\nu_{\text{Fe-imid}}$,op	1.32	$\nu_{FeN_{Im}}(13)+\delta_{C_{m,I}C_1C_{P,I}}(5)+\delta_{C_{m,IV}C_4C_{P,IV}}(6)$
248	$\gamma_9+\nu_{\text{Fe-imid}}$,op	1.75	$\nu_{FeN_{Im}}(21)+\delta_{C_{m,I}C_1C_{P,I}}(7)+\delta_{C_{m,III}C_3C_{P,III}}(6)+\delta_{C_{m,IV}C_4C_{P,IV}}(10)$
288	$\nu_{53,50}$,ip	1.54	$\nu_{FeN_{P,I}}(7)+\nu_{FeN_{P,II}}(15)+\nu_{FeN_{P,III}}(7)+\nu_{FeN_{P,IV}}(14)$
293	$\nu_{53,50}$,ip	1.56	$\nu_{FeN_{P,I}}(15)+\nu_{FeN_{P,II}}(5)+\nu_{FeN_{P,III}}(13)+\nu_{FeN_{P,IV}}(7)$
404	$\nu_{50a,53a}$,ip	0.87	$\nu_{FeN_{P,II}}(13)+\nu_{FeN_{P,IV}}(13)$
406	$\nu_{50b,53b}$,ip	0.92	$\nu_{FeN_{P,I}}(13)+\nu_{FeN_{P,III}}(15)$

that largely preserves the character of a core porphyrin mode will have a large overlap with just one mode. A mode that has significant overlap with multiple porphyrin core modes reflects the deviation from D_{4h} symmetry, and the mixing of imidazole and phenyl modes with the porphyrin core modes.

Table I indicates the extent of overlap of the various best-fit [Fe(TPP)(2-MeHIm)] modes with some of the porphyrin core modes. It also shows the overlap of calculated modes with Fe-N_{im} stretch and Fe-N_{im}-C_{im} angle bend coordinates to identify the Fe modes most affected by the imidazole ligand. The significant overlap of each true [Fe(TPP)(2-MeHIm)] iron mode with so many modes of the porphyrin core demonstrates the limitation of labeling the actual modes in terms of the conventional porphyrin core modes.

Further information on the character of the [Fe(TPP)(2-MeHIm)] modes is obtained from their potential energy distributions (PED), as shown in Table II. For a given mode, the PED describes the contributions of various internal coordinates of the system to its potential energy, and reveals the relative contributions of the phenyl, imidazole, and porphyrin core force constants.

The best-fit calculation is used to characterize the observed iron modes of [Fe(TPP)(2-MeHIm)]. As shown in Figs. 3 and 4, good agreement between the calculated and experimental iron VDOS is achieved over a wide range of frequency. The disagreement between the calculation and the experiment in the low frequency region (below ~ 50 cm^{-1}) is due to our single molecule model of [Fe(TPP)(2-MeHIm)], which does not incorporate intermolecular interactions and crystal field effects that are expected to play important roles at low frequencies. Acoustic modes involving large displacements of iron are likely to contribute to the broad asymmetric feature around 30 cm^{-1}.

Compared to the traditional normal mode calculations,

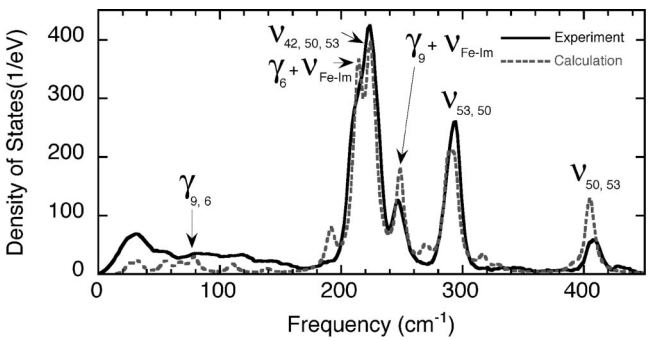

FIG. 3. The measured and calculated Fe vibrational density of states. The calculated VDOS is multiplied by an arbitrary scale factor.

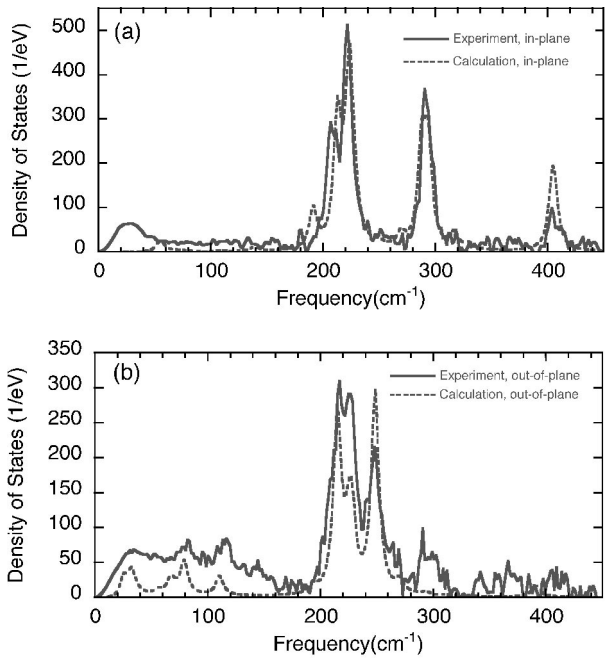

FIG. 4. The measured and calculated Fe vibrational density of states for (a) in-plane (b) and out-of-plane iron modes. The calculated VDOS are multiplied by an arbitrary scale factor.

which are fitted to resonance Raman data and supplemented with various shifts from isotopic substitutions, the calculations that fit to NRVS data have many more experimental constraints on modes that indisputably involve large Fe motions. The frequency, amplitude, and direction of perhaps eight well-resolved NRVS peaks must be reproduced by the calculation, while simultaneously maintaining agreement with another half dozen high frequency modes determined by Raman data. At the same time, however, there are hundreds of unknown force constants, so the calculation is still underdetermined. Inspection of Figs. 3 and 4 reveal several examples of the calculated amplitudes differing noticeably from the measured peaks, and even cases where the frequencies are slightly mismatched. We find that continued tweaking of certain force constants, especially the off-diagonal ones, can gradually lead to better fits. However, at this level such tweaking does not affect the character of the relevant normal modes. It is not clear that continued refinements (without change in the mode characteristics) would be physically meaningful, given the possible uncertainties in the structure and the neglect of interactions between molecules.

The characterization and assignment of the [Fe(TPP)(2-MeHIm)] iron modes can be separated into two categories: vibrations with PEDs largely localized to the porphyrin core, and coupled vibrations of imidazole and the phenyl rings with the porphyrin core. We sort the modes into the following four groups: (a) in-plane vibrations having significant overlap with ν_{42}, ν_{50}, and ν_{53} modes of the porphyrin core; (b) modes with a large contribution from the iron-imidazole stretch coordinate; (c) low frequency modes involving phenyl and imidazole vibrations; and (d) the porphyrin out-of-plane modes.

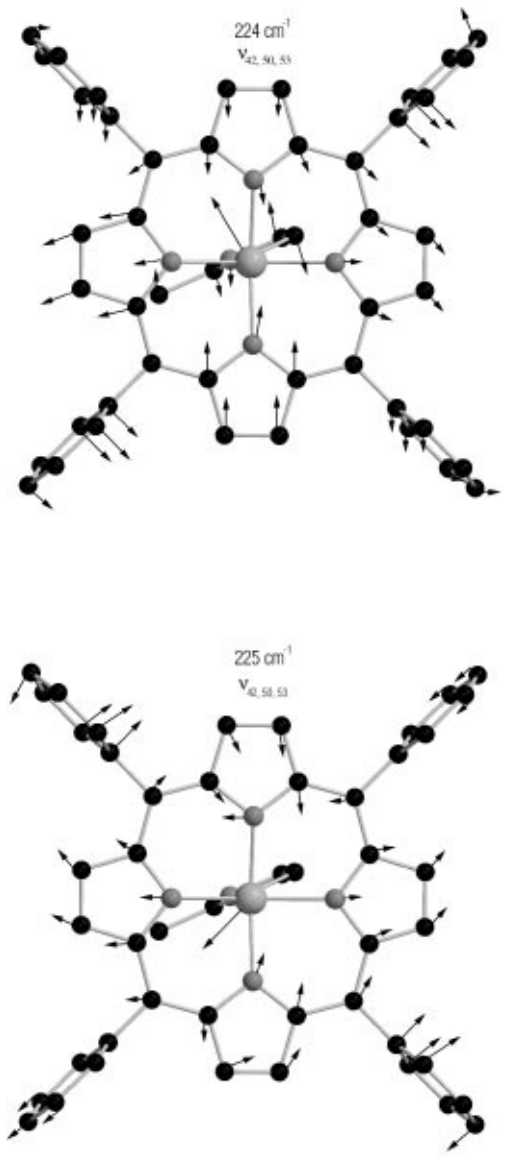

FIG. 5. The eigenvectors of the in-plane modes at 224 and 225 cm^{-1}. These modes show significant overlap with ν_{42}, ν_{50}, and ν_{53} porphyrin core vibrations. The lengths of the arrows indicate relative magnitudes of atom displacements.

A. In-plane porphyrin modes

The group theoretical considerations of the D_{4h} symmetric porphyrin indicate 18 doubly degenerate modes with E_u symmetry [Eq. (4)]. As mentioned earlier, in a fourfold symmetric porphyrin E_u modes involve a nonzero displacement of iron and are Raman inactive. Several of these E_u modes are due to out-of-phase vibrations of iron against a couple of pyrrole atoms. Due to small reduced masses, such modes will occur at higher frequencies (outside the 0–800 cm^{-1} range of NRVS) and will have small displacement of Fe. On the other hand, several other E_u modes (such as ν_{53} and ν_{50}) involve out-of-phase displacements of iron against entire pyrrole rings; such modes will occur with a large displacement of Fe and will have low frequencies as a result of larger reduced masses. These modes can be readily detected by NRVS.

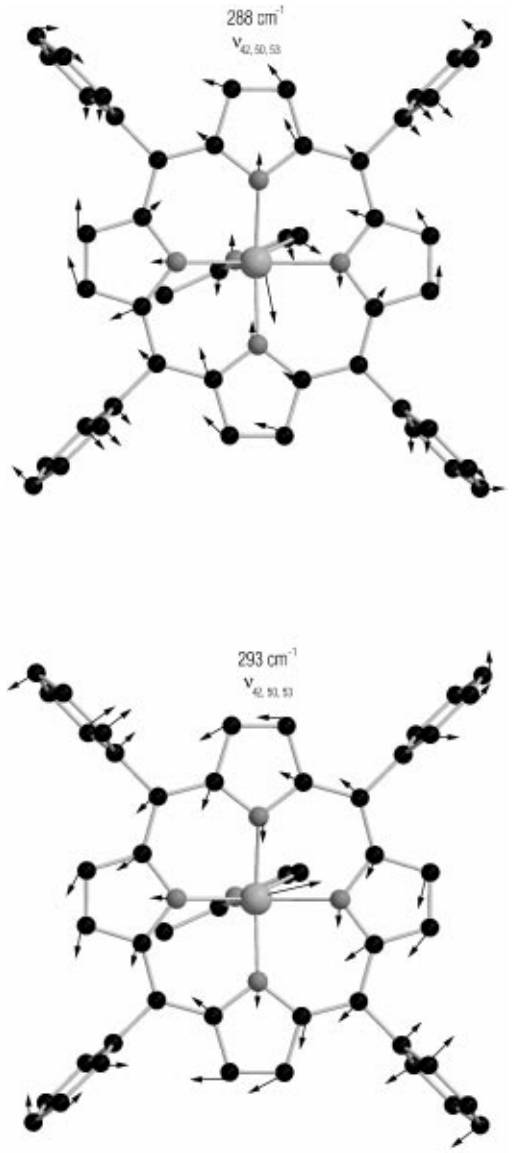

FIG. 6. The eigenvectors of in-plane modes at 288 and 293 cm^{-1}. These modes show significant overlap with ν_{42}, ν_{50}, and ν_{53} porphyrin core vibrations. The lengths of the arrows indicate relative magnitudes of atom displacements.

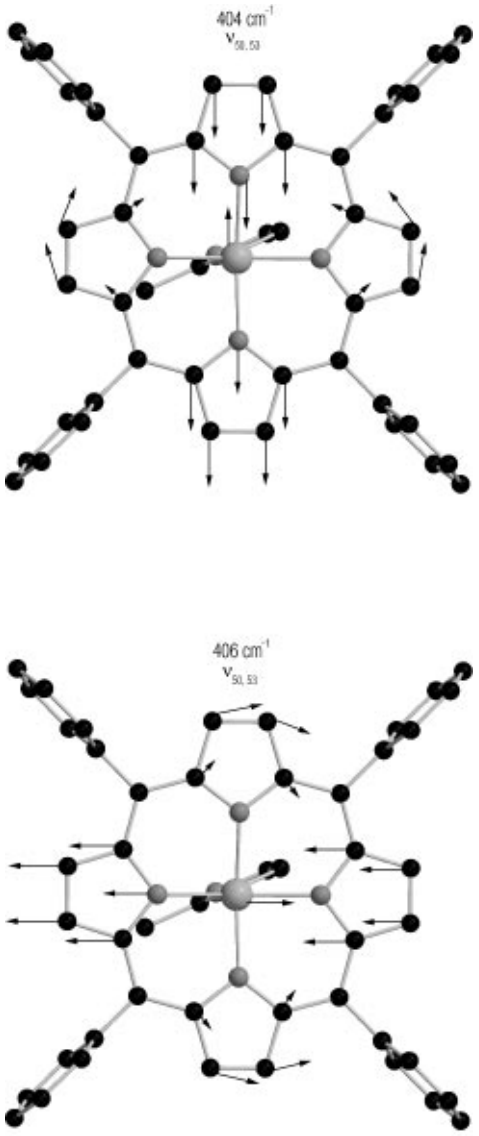

FIG. 7. The eigenvector of $\nu_{50}+\nu_{53}$ modes at 404 and 406 cm^{-1}. The lengths of the arrows indicate relative magnitudes of atom displacements.

Measurements on the oriented crystals of [Fe(TPP)(2-MeHIm)], as shown in Fig. 4(a), indicate the presence of in-plane modes at 205, 220, 290, and 400 cm^{-1}. In addition, at the lowest frequency (30 cm^{-1}) a band having in-plane displacement of iron is observed. The peaks at 220, 290, and 400 cm^{-1} are broad, and each is found to be a superposition of two or more normal modes with nearly equal frequencies, and substantial overlap with the ν_{42}, ν_{50}, and ν_{53} porphyrin core modes. The peak near 220 cm^{-1} is decomposed into overlapping modes at 222, 224, and 225 cm^{-1} [Fig. 4(a)]. The eigenvectors of the modes at 224 and 225 cm^{-1} are shown in Fig. 5. As shown in Table I, all three of these have substantial contributions from the ν_{42}, ν_{50}, and ν_{53} porphyrin core modes. There is no justification for following the usual practice of assigning specific porphyrin core mode labels to any of these peaks, as they are so thoroughly hybridized by the phenyl and imidazole substituents that the porphyrin core no longer provides a good basis set for the normal modes.

The peak near 290 cm^{-1} is composed of two modes that also strongly overlap with the ν_{42}, ν_{50}, and ν_{53} porphyrin core modes. The 405 cm^{-1} peak is also a doublet, but these are primarily admixtures of only two porphyrin core modes, the ν_{50} and ν_{53} modes. The doublets arise simply because the imidazole ring breaks the fourfold rotational symmetry of the molecule. The displacements associated with these modes are illustrated in Figs. 6 and 7.

We can compare the in-plane behavior of this imidazole complex with the similar NO-ligated FeTPP molecule [11]. The primary in-plane features are similar: 242, 322, and

TABLE III. A comparison of Fe-N_P bond lengths and force constants of [Fe(TPP)(2-MeImH)] and [Fe(TPP)(NO)]. The average Fe-N_P bond length of [Fe(TPP)(2-MeImH)] is larger than that of [Fe(TPP)(NO)]. The larger Fe-N_P bond length in [Fe(TPP)(2-MeImH)] causes a softening of the Fe-N_P force constants, which in turn results in smaller frequencies for the ν_{53} modes, for example. The differences in the ν_{53} mode frequencies in [Fe(TPP)(2-MeImH)] (288 and 294 cm^{-1}) and [Fe(TPP)(NO)] (312 and 333 cm^{-1}) is therefore directly related to the variations in the core sizes of the two compounds.

	Bond length (Å)		Force constant (mdyne/Å)	
	[Fe(TPP)(2-MeHIm)][a]	[Fe(TPP)(NO)][b]	[Fe(TPP)(2-MeHIm)][c,d]	[Fe(TPP)(NO)][e]
Fe-$N_{P,I}$	2.063	2.004	1.24	1.35
Fe-$N_{P,II}$	2.068	1.977	1.20	1.49
Fe-$N_{P,III}$	2.079	2.027	1.24	1.35
Fe-$N_{P,IV}$	2.083	1.977	1.20	1.49

[a]Reference [19].
[b]Reference [37].
[c]This Work.
[d]A complete list of force constants is available from the authors.
[e]Reference [11].

405 cm^{-1} peaks for NO, and 230, 290, and 405 cm^{-1} for imidazole. While mixing of the ν_{42}, ν_{50}, and ν_{53} porphyrin core modes is also seen with the NO ligand, the imidazole produces substantially more mixing. This is likely due to the lower symmetry of the imidazole complex.

The ν_{53} modes (312 and 333 cm^{-1}) of [FeTPP(NO)] show a large splitting of about 20 cm^{-1} due to strong coupling with the NO ligand. In addition, the ν_{53} doublet in [Fe(TPP)(NO)] occurs at higher frequencies compared to the doublet (288 and 293 cm^{-1}) in [Fe(TPP)(2-MeHIm)]. The largest contribution to the PEDs of the ν_{53} modes comes from the Fe-N_P internal coordinates (Table II). Therefore, we observe a softening of the Fe-N_P force constants in [Fe(TPP)(2-MeHIm)] associated with the smaller values of the ν_{53} frequencies in this compound compared to that in [Fe(TPP)(NO)]. This observation is related to the differences in the structures of the two compounds under consideration. The x-ray measurements show a larger average Fe-N_P bond length for [Fe(TPP)(2-MeHIm)] than that for [Fe(TPP)(NO)]. Table III compares the bond length and force constants of the four Fe-N_P bonds of [Fe(TPP)(2-MeHIm)] and [Fe(TPP)(NO)], and demonstrates the correlation between larger bond length and smaller force constant.

B. Iron-imidazole vibrations

The iron-imidazole stretch mode ($\nu_{\text{Fe-im}}$) is Raman active in the deoxy state of Mb, Hb, and various heme model compounds. Resonant enhancement through coupling with an electronic transition (Soret band) gives rise to a strong Raman peak near 220 cm^{-1} [29,5]. The first reports of identifying this mode in Mb, Hb, and several model compounds were rather ambiguous [6,30]. Subsequently, Argade *et al.* confirmed the assignment of the iron-imidazole stretch mode in deoxy-Mb by using isotope substitution of Fe [7]. The $\nu_{\text{Fe-His}}$ band in deoxy-Mb and Hb has been widely studied, and the frequency and Raman intensity of this mode are found to be sensitive to the global protein structure [31–33]. A decomposition of the $\nu_{\text{Fe-His}}$ Raman band profile in deoxymyoglobin into several spectral lines has been used to infer the relative population of the major conformational substates [31–33]. Locally, the iron-imidazole stretch mode is found to be sensitive to three coordinates: the extent of doming of the iron atom from the mean heme plane, the off-axial tilt of iron-imidazole bond from the heme normal, and the azimuthal angle of the imidazole plane [34].

The [Fe(TPP)(2-MeHIm)] single-crystal data show two distinct out-of-plane modes at 214 and 225 cm^{-1} (Fig. 2), close to the iron-histidine mode in deoxy-Mb [7]. Our calculation yields out-of-plane modes at 215 and 228 cm^{-1}, in excellent agreement with the data [Fig. 4(b)]. The 215 cm^{-1} mode has a large PED contribution (35%) from the iron-imidazole stretch force constant (Table II), and large overlaps with the γ_6 porphyrin core mode as well as the Fe-imidazole stretch mode. The 228 cm^{-1} mode has a strong overlap with the γ_9 porphyrin core mode, plus the Fe-imidazole stretch.

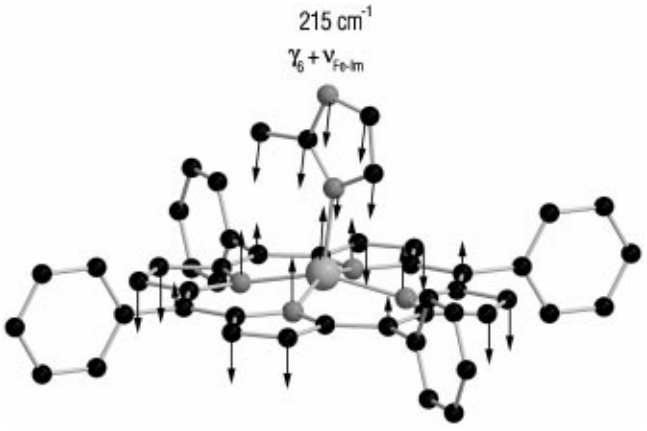

FIG. 8. The eigenvector of the out-of-plane iron-imidazole stretch mode at 215 cm^{-1}. This mode also has a large overlap with out-of-plane γ_6 vibration. The lengths of the arrows indicate relative magnitudes of atom displacements.

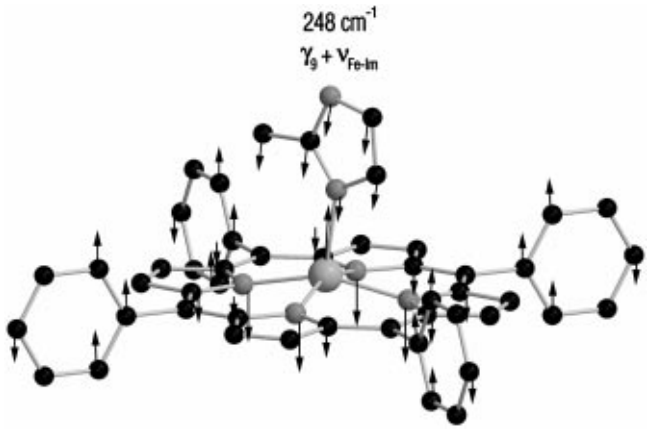

FIG. 9. The eigenvector of the out-of-plane iron-imidazole stretch mode at 248 cm^{-1}. This mode also has a large overlap with γ_9 doming vibration. The lengths of the arrows indicate relative magnitudes of atom displacements.

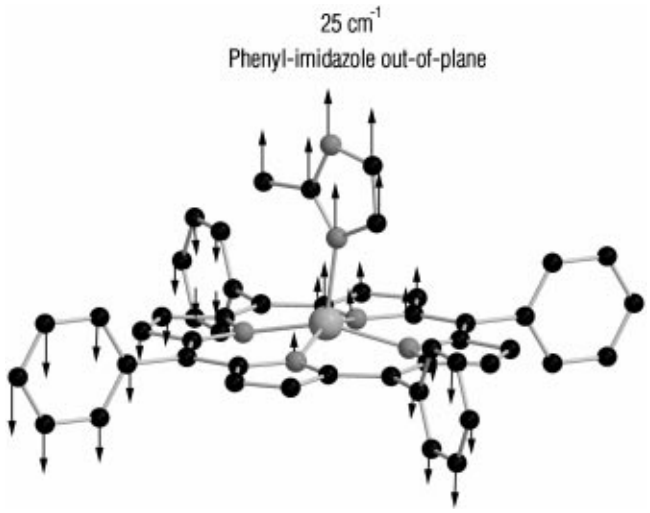

FIG. 10. The eigenvector of the phenyl out-of-plane mode at 25 cm^{-1}. The lengths of the arrows indicate relative magnitudes of atom displacements.

The displacements associated with the 215 cm^{-1} modes are shown in Fig. 8.

The measured spectrum also clearly shows an out-of-plane mode at 248 cm^{-1}. Peaks near this frequency have been seen in Raman measurements on deoxy-Mb, including those by Argade and co-workers [7]. No shift of this peak was seen upon Fe isotope substitution, however, suggesting that no significant Fe motion is involved. On the contrary, the NRVS unambiguously shows this mode to have a substantial iron displacement. The normal mode analysis shows a mixed character mostly involving the iron-imidazole stretch and doming (γ_9) coordinates (see Fig. 9). Upon substitution of ^{54}Fe with ^{57}Fe in the calculation, this mode shifts by 1.2 cm^{-1}. The corresponding shift in deoxy-Mb may have been smaller and below the experimental resolution [7]. Clearly, NRVS is capable of identifying Raman-active modes with Fe contributions that are difficult to determine by other means.

The bending motion of the imidazole ligand is associated with the out-of-plane mode at 110 cm^{-1}. This mode has a 44% overlap with the Fe-imidazole bending coordinate and it also involves a small doming and pyrrole tilting motion of the porphyrin core. Imidazole bending also contributes to the low frequency phenyl modes, discussed below.

C. Phenyl modes

The modes with the largest amplitude Fe motions are due to coupling of the phenyl rings to the porphyrin core. The force constants that produce the best fit to the data at higher frequencies also yield a series of such phenyl modes at 25, 32, 33, 54, and 56 cm^{-1}. The eigenvector of one of these modes at 25 cm^{-1} is shown in Fig. 10. Table II includes the calculated Fe amplitudes, showing displacements for the 25 and 33 cm^{-1} modes (3.45 and 2.11 pm) significantly larger than for any other mode. Computer animation of the motions described by the normal mode eigenvectors dramatically confirms the role of the phenyl rings in causing large doming displacements of the entire molecule. Examination of the PEDs in Table II reveals that the Fe displacement is also accompanied by a bending of the imidazole ring. In other words, the most significant doming motion of the porphyrin core is actually caused by the coupling of the phenyl substituents on the periphery of the molecule, and by the imidazole ring bound to the central Fe atom. These two features, of course, would be overlooked in any calculation of porphyrin core modes. These results suggest that not only are the porphyrin core normal modes a poor basis set for the true modes of this molecule, but they also neglect the features that may be of the greatest biological significance.

There is one caveat regarding the low frequency modes. As previously noted, the calculation assumes a single molecule with no coupling to any neighbors. This will necessarily omit contributions from intermolecular coupling, crystal fields, and acoustic mode dispersion. These are most important in the low frequency regime occupied by the phenyl modes. It is clear from Fig. 4 that the calculations do not yield all of the low frequency modes. There appears to be a continuum in the out-of-plane modes up to about 150 cm^{-1}, with several identifiable peaks that correspond to calculated modes [Fig. 4(b)].

D. Porphyrin out-of-plane modes

Heme out-of-plane modes are biologically significant as they are expected to be central to the dynamics of ligand binding and dissociation in heme proteins. The modes of particular interest are those involving large iron displacement perpendicular to the heme plane, as ligand binding is also associated with such displacements. As noted earlier, only the Raman inactive A_{2u} modes of the fourfold symmetric porphyrin involve significant out-of-plane motion of iron. Such modes are also difficult to identify with IR spectroscopy, since it is hard to distinguish heme modes from the more numerous protein modes.

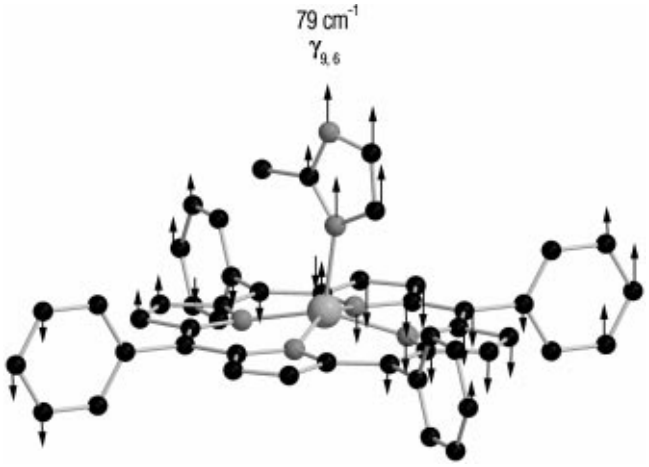

FIG. 11. The eigenvector of the out-of-plane doming (γ_9) mode at 79 cm^{-1}. The lengths of the arrows indicate relative magnitudes of atom displacements.

Using femtosecond coherence spectroscopy, Zhu *et al.* identified a doming mode in deoxymyoglobin at 50 cm^{-1} [35]. In a subsequent study, Rosca *et al.* reported a low frequency feature at 40 cm^{-1} in myoglobin with an NO ligand, which they identified as a doming mode [36].

In a recent NRVS study, Rai *et al.* observed the iron out-of-plane modes in the 5-coordinated model heme compound [Fe(TPP)(NO)] [11], with modes at 74 and 128 cm^{-1} assigned primarily to the doming (γ_9) and pyrrole (γ_6) tilting vibrations of porphyrin. The γ_9 and γ_6 modes also contribute significantly to higher frequency modes involving ligand vibrations. Again, the largest doming displacement is found in a 32 cm^{-1} phenyl mode.

The present study of [Fe(TPP)(2-MeHIm)] finds three porphyrin modes with out-of-plane displacements of iron, at 67, 79, and 110 cm^{-1}. These modes are significantly delocalized over the porphyrin core and show some coupling with the imidazole vibrations. The 110 cm^{-1} mode involves a strong Fe-imidazole bending motion, while the 67 and 79 cm^{-1} modes have large overlaps with γ_9 doming and γ_6 pyrrole tilting coordinates (29% and 40%, respectively, with the γ_9 mode, and 15% and 23%, respectively, with γ_6). Figure 11 shows the character of the 79 cm^{-1} mode. While we have identified the normal mode with the largest overlap with the porphyrin core doming modes, greater doming displacements belong to the low frequency phenyl modes (e.g., 3.45 pm at 25 cm^{-1} vs 1.51 pm at 79 cm^{-1}).

V. CONCLUSIONS

Normal mode analysis of NRVS data from [Fe(TPP)(2-MeHIm)] has provided a wealth of insights into the detailed Fe dynamics for this compound, which is a model for the active center in deoxy forms of myoglobin, hemoglobin, and related proteins. The NRVS data provide constraints on the frequencies, amplitudes, and directions of many modes with large Fe motions, which provides a much higher level of confidence in the output of the computations. The orientation-dependent data from a single-crystal specimen, which relies on the sensitivity of nuclear resonant absorption only to Fe motions in the direction of the incident x-ray beam, has provided directional information on individual modes. These constraints are combined with previous Raman results on high frequency modes to arrive at a best-fit set of force constants that reproduce all of these data, and give a complete description of the eigenvectors of motion.

A general feature of all the results is that the actual normal modes do not map well onto the normal modes of the porphyrin core. Conventional studies based on Raman peaks have traditionally labeled the peaks according to these porphyrin core modes, but the greater sensitivity and Fe selectivity of the NRVS data yields calculated modes of sufficient quality that the severe limitations of the porphyrin core modes is apparent.

The major in-plane modes are admixtures of various porphyrin core modes, occurring near 220, 290, and 400 cm^{-1}. These results show a splitting of core modes, which are caused by the imidazole lifting the fourfold rotational symmetry of the porphyrin core. A similar array of split peaks was observed in the related nitrosyl compound, Fe(TPP)(NO) [11]. The frequency shifts in going from the nitrosyl to the imidazole compound follow from the observed correlation between longer Fe-N_P bond lengths and smaller stretch force constants.

The various force constants connecting Fe with the imidazole ring make significant contributions to the normal modes at 215, 228, and 248 cm^{-1}. The first two are in good agreement with the Fe-His modes assigned to deoxy-Mb and related heme structures. The third mode, however, has been observed in Raman spectroscopy but not assigned to Fe motion. The definitive assignment of the 248 cm^{-1} peak to an out-of-plane Fe-imidazole mode demonstrates the greater sensitivity to Fe motions than previously possible with combined Raman-isotope shift studies.

Perhaps the most important conclusion is that the outer phenyl substituents, in concert with the imidazole, lead to doming modes with the greatest displacement of the Fe atom. These modes are important to understand the dynamics of ligand binding, which is accompanied by Fe out-of-plane displacements. These results confirm the role of substituents in driving the low frequency doming modes. The traditional doming modes of the porphyrin core have also been identified here, at 67, 79, and 110 cm^{-1}, but their displacements are smaller than those of several phenyl modes.

ACKNOWLEDGMENTS

This work was supported by the National Science Foundation through Grant No. PHY-9988763 (for authors B.K.R., S.D., and E.W.P.) and Grant No. PHY-9983100 (J.T.S.), and by the National Institutes of Health Grant Nos. GM-28401 (M.K.E. and W.R.S.) and GM-52002 (J.T.S.). Support from the Mobile Manufacturers Forum (B.K.R. and E.W.P.) and from the Purdue Research Foundation (B.K.R.) is gratefully acknowledged. Use of the Advanced Photon Source was supported by the U.S. Department of Energy, Basic Energy Sciences, Office of Science, under Contract No. W-31-109-Eng-38.

[1] L. Stryer, *Biochemistry,* 3rd ed. (Freeman, New York, 1988).
[2] G. Fermi, in *Molecular Structures in Biology*, edited by R. Diamond *et al.* (Oxford University Press, New York, 1993), Chap. 6, pp. 164–191.
[3] T.G. Spiro and X.Y. Li, in *Bilogical Application of Raman Spectroscopy*, edited by T.G. Spiro (Wiley, New York, 1988), Vol. 3, Chap. 1, pp. 1–37.
[4] A.D. Procyk and D.F. Bocian, Annu. Rev. Phys. Chem. **43**, 465 (1992).
[5] J.R. Kincaid, in *The Porphyrin Handbook*, edited by K.M. Kadish, K.M. Smith, and R. Guilard (Academic Press, New York, 2000), Vol. 7, Chap. 5, pp. 225–291.
[6] H. Hori and T. Kitagawa, J. Am. Chem. Soc. **102**, 3608 (1980).
[7] P.V. Argade, M. Sassaroli, D.L. Rousseau, T. Inubushi, M. Ikeda-Saito, and A. Lapidot, J. Am. Chem. Soc. **106**, 6593 (1984).
[8] M. Seto, Y. Yoda, S. Kikuta, X.W. Zhang, and M. Ando, Phys. Rev. Lett. **74**, 3828 (1995).
[9] W. Sturhahn, T.S. Toellner, E.E. Alp, X. Zhang, M. Ando, Y. Yoda, S. Kikuta, M. Seto, C.W. Kimball, and B. Dabrowski, Phys. Rev. Lett. **74**, 3832 (1995).
[10] W. Sturhahn and V.G. Kohn, Hyperfine Interact. **123**, 367 (1999).
[11] B.K. Rai, S.M. Durbin, E.W. Prohofsky, J.T. Sage, G.R.A. Wyllie, W.R. Scheidt, W. Sturhahn, and E.E. Alp, Biophys. J. **82**, 2951 (2002).
[12] J.T. Sage, C. Paxson, G.R.A. Wyllie, W. Sturhahn, S.M. Durbin, P.M. Champion, E.E. Alp, and W.R. Scheidt, J. Phys.: Condens. Matter **13**, 7707 (2001).
[13] J.T. Sage, S.M. Durbin, W. Sturhahn, D.C. Wharton, P.M. Champion, P. Hession, J. Sutter, and E.E. Alp, Phys. Rev. Lett. **86**, 4966 (2001).
[14] K. Achterhold *et al.*, Phys. Rev. E **65**, 051916 (2002).
[15] A.D. Adler, F.R. Longo, J.D. Finarelli, J. Goldmacher, J. Assour, and L. Korsakoff, J. Org. Chem. **32**, 476 (1967).
[16] M. Landergren and L. Baltzer, Inorg. Chem. **29**, 556 (1990).
[17] E.B. Fleischer and T.S. Srivastava, J. Am. Chem. Soc. **91**, 2403 (1969); A.B. Hoffman, D.M. Collins, V.W. Day, E.B. Fleischer, T.S. Srivasatva, and J.L. Hoard, *ibid.* **94**, 3620 (1972).
[18] A.M. Stolzenberg, S.H. Strauss, and R.H. Holm, J. Am. Chem. Soc. **103**, 4763 (1981).
[19] M.K. Ellison, C.E. Schulz, and W.R. Scheidt, Inorg. Chem. **41**, 2173 (2002).
[20] C. Keppler *et al.*, Eur. Biophys. J. **25**, 221 (1997).
[21] A.I. Chumakov and W. Sturhahn, Hyperfine Interact. **123**, 781 (1999).
[22] E.B. Wilson, J.C. Decius, and P.C. Cross, *Molecular Vibrations* (McGraw-Hill, New York, 1955).
[23] T.S. Rush, III, P.M. Kozlowski, C.A. Piffat, R. Kumble, M.Z. Zgierski, and T.G. Spiro, J. Phys. Chem. B **104**, 5020 (2000).
[24] J.M. Eyster, Ph.D. thesis, Purdue University, 1974 (unpublished).
[25] I.W. Levin, in *Vibrational Spectra and Structure*, edited by J.R. Durig (Elsevier Scientific, New York, 1975), Vol. 4, pp. 102–186.
[26] K.S. Singwi and A. Sjölander, Phys. Rev. **120**, 1093 (1960).
[27] H. Paulsen, H. Winkler, A.X. Trautwein, H. Grünsteudel, V. Rusanov, and H. Toftlund, Phys. Rev. B **59**, 975 (1999).
[28] M. Abe, T. Kitagawa, and Y. Kyogoku, J. Chem. Phys. **69**, 4526 (1978).
[29] T. Kitagawa, in *Bilogical Application of Raman Spectroscopy*, edited by T.G. Spiro (Wiley, New York, 1988), Vol. 3, Chap. 3, pp. 97–131.
[30] A. Desbois, M. Lutz, and R. Banerjee, Biochemistry **18**, 1510 (1979).
[31] M. Bosenbeck, R. Schweitzer-Stenner, and W. Dreybrodt, Biophys. J. **61**, 31 (1992).
[32] H. Gilch, W. Dreybrodt, and R. Schweitzer-Stenner, Biophys. J. **69**, 214 (1995).
[33] H. Gilch, R. Schweitzer-Stenner, and W. Dreybrodt, Biophys. J. **65**, 1470 (1993).
[34] S.S. Stavrov, Biophys. J. **65**, 1942 (1993).
[35] L. Zhu, P. Li, M. Huang, J.T. Sage, and P.M. Champion, Phys. Rev. Lett. **72**, 301 (1994).
[36] F. Rosca, A.T.N. Kumar, X. Ye, T. Sjodin, A.A. Demidov, and P.M. Champion, J. Phys. Chem. A **104**, 4280 (2000).
[37] W.R. Scheidt, H.F. Duval, T.J. Neal, and M.K. Ellison, J. Am. Chem. Soc. **122**, 4651 (2000).